Thin-wall injection molding of polypropylene using molds with different laser-induced periodic surface structures

Masato, Davide; Sorgato, Marco; Batal, Afif; Dimov, Stefan; Lucchetta, Giovanni

DOI:
10.1002/pen.25189

Slip of polypropylene melts over different laser-induced periodic nano-structures in thin-wall injection molding

D. Masato[a, †], *M. Sorgato*[b], *A. Batal*[c], *S. Dimov*[c], *G. Lucchetta*[b]

[a] Department of Plastics Engineering, University of Massachusetts Lowell, One University Ave, Lowell, MA, United States

[a] Department of Industrial Engineering, University of Padova, via Venezia 1, Padova, Italy

[b] Department of Mechanical Engineering, University of Birmingham, Birmingham, UK

[†] corresponding author, davide_masato@uml.edu, +19789342836

Slip of polypropylene melts over different laser-induced periodic nano-structures in thin-wall injection molding

D. Masato, M. Sorgato, A. Batal, S. Dimov, G. Lucchetta

Abstract. In injection molding, high pressure is required to completely replicate the mold geometry, due to the viscosity of thermoplastic polymers, the reduced thickness of the cavity and the low mold temperature. The reduction of the drag required to fill a thin-wall injection molding cavity can be promoted by inducing the strong slip of the polymer melt over the mold surface, which occurs within the first monolayer of macromolecules adsorbed at the wall. In this work, the effects of different Laser-Induced Periodic Surface Structures (LIPSS) topographies on the reduction of the melt flow resistance of polypropylene were characterized. Ultrafast laser processing of the mold surface was used to manufacture nano-scale ripples with different orientation and morphology. Moreover, the effects of those injection molding parameters that mostly affect the interaction between the mold surface and the molten polymer were evaluated. The effect of LIPSS on the slip of the polymer melt was modelled to understand the effect of the different treatments on the pressure required to fill the thin-wall cavity. The results show that LIPPS can used to treat injection mold surfaces to promote the onset of wall slip, thus reducing the injection pressure up to 13%.

Keywords: thin-wall injection molding; laser-induced periodic surface structures; wall-slip; reduction of melt flow resistance; mold surface engineering

1. Introduction

The interest for weight and cost reduction of plastic products has been constantly pushing injection molding manufactures towards the design of thinner parts [1-3], thus allowing the reduction of resources consumption and of the environmental burdens [4]. In this context, the capabilities of the injection molding process have to be developed to sustain the trend towards cavity thickness reduction while maintaining the quality standards [5]. In this sense, engineering of mold surface topography for injection molding of thin-wall plastics parts is of great interest for several plastic manufacturing applications, as packaging, consumer electronics and biomedics [6].

Design and optimization of mold surface properties can lead to improvements of the filling phase of thin-wall cavities, which is the most critical phase of the process due to the raise of cavity pressure [7]. In fact, mold surface properties can be exploited to minimize the interactions between the polymer and the tool thus reducing the pressure required to achieve complete replication of the mold geometry [8]. Recently, Masato et al. observed that low-friction mold surface coatings can be used to promote the filling behavior of polystyrene injected in thin-wall cavities through the wall slip phenomena at the polymer-mold interface [9]. In fact, the reduced thickness typical of thin-wall parts can lead to polymer flows characterized by shear stress values significantly higher than those observed in conventional injection molding [10]. Under these flow conditions, the conventional 'no-slip boundary condition' is no longer valid and the onset of the wall slip phenomenon occurs [11].

Considering a polymer melt flowing next to a solid wall polymer, it can be assumed that a monolayer exists where macromolecular chains are adsorbed to the wall through several sites along their backbone [12]. These molecules are connected with the bulk of the polymer through entanglements with other neighbor molecules. Under flow conditions, the chain loops attached to the mold surface are pulled by the entanglements with the bulk molecules that are being stretched in the flow direction. When the applied forces increase above a critical value, the chains detach from the interface, leading to the onset of wall slip [13].

Several researchers have reported that surface topography have a significant effect on the wall slip phenomenon [14-16]. Ebrahimi et al. investigated the slip of polymer melts over micro-patterned metallic surfaces under isothermal temperature conditions [12]. The surface of the dies were manufactured by laser irradiation, to obtain topographies characterized by roughness values in the range of few micrometers, thus being much larger

than the coil size of a typical polymer macromolecular chain that is of the order of a few nanometers. Consequently, when flowing through the die, the polymer chains replicate the topography and the polymer-wall interface is replaced by a stronger polymer-polymer interface, which leads to a decrease of the wall-slip phenomenon.

In contrast, Bellantone et al. performed short-shot injection molding experiments observing that, as cavity thickness decreases, higher surface roughness allows the melt to flow forward into the cavity [17]. Similar results were found Zhang et al. that developed a model to predict the effect of surface roughness and reported that it affects the filling behavior by modifying the heat transfer mechanism at the polymer-mold interface [18]. However, in both studies the mold surface was realized by means of conventional machining processes and the roughness of the mold surface was in the micrometer range.

Laser Induced Periodic Surface Structures (LIPSS) are well known surface nano-structures that are generated with linearly polarized laser using ultrashort pulse [19]. The ablation with femtosecond-lasers generates topographies characterized by periodic nano-structured ripples that were recently used to modify the surface properties for an increasing number of applications [20]. In particular, LIPSS have been successfully used to modify the wettability of steel surfaces [21,22], improve their tribological behavior [23] and increase hardness and wear resistance [24,25].

In injection molding applications, femtosecond-laser processing has been used to functionalize the surfaces of plastic parts by treating the mold surfaces [26,27]. In particular, Bekesi et al. utilised a short-pulse laser to pattern/texture the surfaces of injection molds that were used to produce polymer replicas with super-hydrophobic surfaces [28]. Jwad et al. exploited the use of laser-induced ripples to fabricate diffraction holograms, which could potentially be transferred onto plastic parts and mass manufactured by injection molding [29]. To replicate completely such nano-scale structures, the temperature of the mold surface must be higher than the polymer glass transition temperature (for amorphous polymers) or melting temperature (for semi crystalline ones) [30,31]. More recently, LIPSS with the same morphology but different orientation were used to reduce the melt flow resistance of polyethylene terephthalate (PET) injected in a slit die cavity [32]. The results were encouraging but the effect needs further investigation, especially regarding the influence of ripples' morphology and injection molding conditions.

In this work, the pressure required to fill a thin-wall injection molding cavity was analyzed considering the effects of different LIPSS topographies. Three different ripples' orientations and morphologies were obtained by controlling the direction of the laser polarization plane. The wall slip behavior of a polypropylene melt injected over nano-structured mold surfaces was characterized under non-isothermal temperature conditions. The effects of process parameters on interactions between the mold surface and molten polymer were investigated, i.e. mold temperature and injection speed. A numerical model of the injection molding process was then used to determine the slip velocity and thus to understand better the effects of LIPSS on reducing the melt flow resistance.

2. Materials and methods

2.1. Part and mold design

In this study, the effect of LIPSS on the filling flow resistance was investigated by monitoring the pressure drop of the polymer melt in a thin-wall injection molding cavity. Specifically, two piezoelectric transducers were flush mounted into the cavity and thus to obtain direct measurements of the cavity pressure drops on each laser treatmented mold surface.

Injection molding experiments were conducted using a slit die geometry of the mold cavity, which had a length (L) of 40 mm, width (w) of 6 mm and thickness (t) of 0.4 mm. The open-flow channel design allows a stationary flow regime to be achieved under injection molding conditions [33]. In fact, when the flow front reaches the end of the channel the injection pressure stabilizes to a steady-state value.

A modular mold assembly (Hasco K-standard system) was designed to mount interchangeable inserts with different LIPSS on both sides of the cavity, as shown in Fig. 1. The mold temperature was set and controlled using two electrical cartridge heaters (diameter: 6.5 mm) and a thermocouple in each of the mold halves.

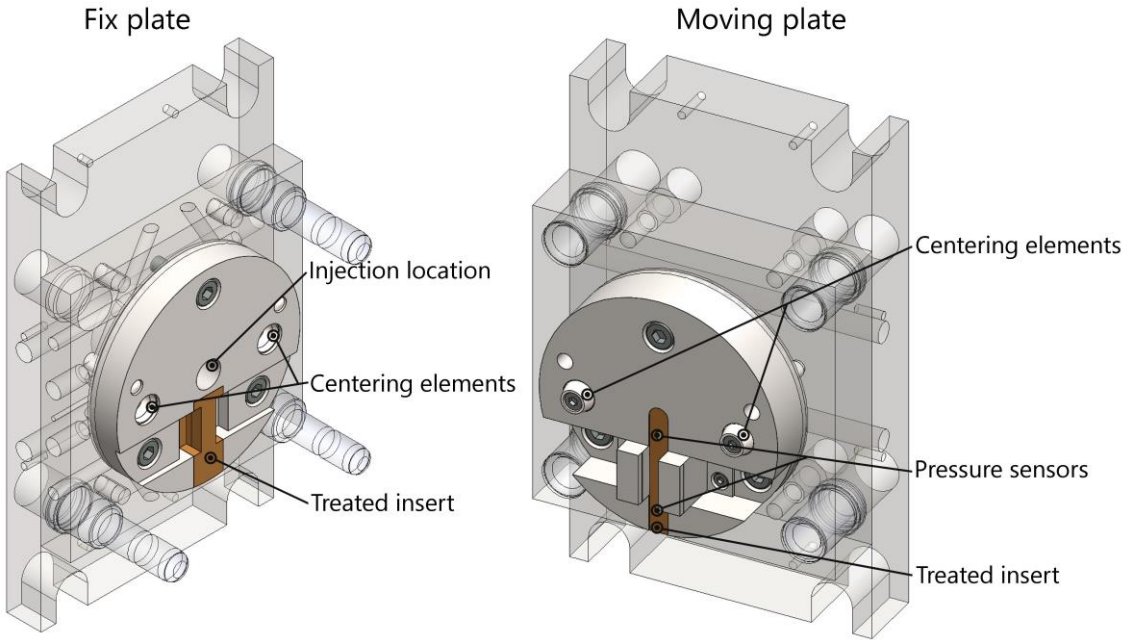

Fig. 1. Mold design with the treated inserts used for the injection molding experiments

2.2. LIPSS generation

The mold inserts were treated using an ultrashort laser to generate LIPSS on steel surfaces. In particular, nano-scale ripples on the mold cavity walls were obtained by processing the surfaces with a near-infrared ultrashort laser with a wavelength of 1030 nm. Before the laser processing, the steel (hardened and tempered H13 chromium-molybdenum) surfaces of the mold inserts were polished to obtain a surface roughness (*Sa*) better than 0.2 µm. Table 1 provides the main process settings used for covering the mold inserts with LIPSS.

Table 1. Process parameters used to generate LIPSS on the mold insert surfaces.

Insert #	Laser Fluence [J/cm^2]	LIPSS Direction	Pulse Duration [fs]	Repetition Rate [kHz]	Scanning Speed [mm/s]
1	0.161	∥	310	250	1000
2	0.161	⊥	310	250	1000
3	0.161 & 0.028	∥ & ⊥	310	250	1000

Three different nano-structured topographies were obtained by generation of LIPSS with different morphology and orientation. In particular, Insert 1 and Insert 2 were designed to have identical morphology but different

orientation with respect to the polymer melt flow direction. In fact, when scanning with laser, LIPSS self-organize on the surface with orientation perpendicular to the polarization plane direction [19]. Thus, Insert 1 was treated using a polarization plane with direction perpendicular to the flow direction, allowing the generation of LIPSS parallel (∥) to the flow direction. Conversely, Insert 2 was treated with a polarization plane that had direction parallel to the flow direction and the generated LIPSS were perpendicular (⊥) to the flow direction.

The morphology of the nano-structures realized on Insert 3 was modified by carrying out two consecutive laser scans perpendicular each other.

2.3. LIPSS Characterization

The morphology of the nano-structures generated on the mold cavity surfaces was analyzed by using Scanning Electron Microscopy (SEM – FEI, Quanta 400). Especially, LIPSS on the three inserts were compared and their overall regularity was evaluated. SEM micrographs of the mold inserts surfaces were obtained with an acceleration voltage of 20kV, a working distance of about 10 mm and a secondary and back-scattered electron detector (Everhart-Thornley detector – ETD).

The topography was characterized by employing Atomic Force Microscopy (AFM – Veeco Digital Instruments, CP II). The instrument was equipped with a silicon sharp tip, which had curvature radius of 6 nm, cantilever length of 125 μm, width of 30 μm and thickness of 2 μm.

2.4. Injection molding setup

The effects of LIPSS on the injection molding process were investigated using a commercial polypropylene (PP – Total, PPC 7642). Its properties are provided in Table 2. The polymer was selected because of its wide use in thin-wall applications.

Table 2. Main properties of the polypropylene selected for the injection molding experiments.

Property	Test Method	PP

Structure	-	Crystalline
Density [g/cm^3]	ISO 1183	0.91
Transition temperature [°C]	ISO 6721	165
Melt Volume Rate [cm^3/10 min]	ISO 1133	16 (230 °C – 2.16 kg)

Injection molding experiments were conducted using a state-of-the-art micro injection molding machine (Wittmann Battenfeld, MicroPower 15). The setup allowed a maximum injection speed of 750 mm/s (i.e. a flow rate of about 15 cm^3/s, given the 5 mm diameter of the injection plunger) and a maximum injection pressure of 270 MPa.

2.5. Process monitoring

The melt flow resistance associated with each mold insert, treated with different LIPSS, was investigated by monitoring the cavity pressure drop during the injection phase. Specifically, two piezoelectric transducers (Kistler, 6182C) were used to monitor the pressure at 6 mm and 30 mm from the injection location, respectively. The piezoelectric charge signals from the sensors were acquired, processed and logged using a charge amplifier (Kistler, 5039A), a 16-bit analog input module (National Instruments, NI 9205) and a software created in Labview. The acquisitions were performed at a rate of 2,500 s^{-1} (i.e. with a time step of 0.4 ms).

The acquired cavity pressure curves were aligned to the beginning of the injection phase, and the steady-state values of the cavity pressure were collected (Fig. 2). The melt flow resistance was then evaluated by calculating the difference between the average values of the steady–state zones of the two pressure signals (i.e. gate pressure, end pressure). In fact, the difference between the pressure values measured at the two extremities of the channel represents the resulting pressure drop in the mold cavity, which was selected as the response variable for the analysis.

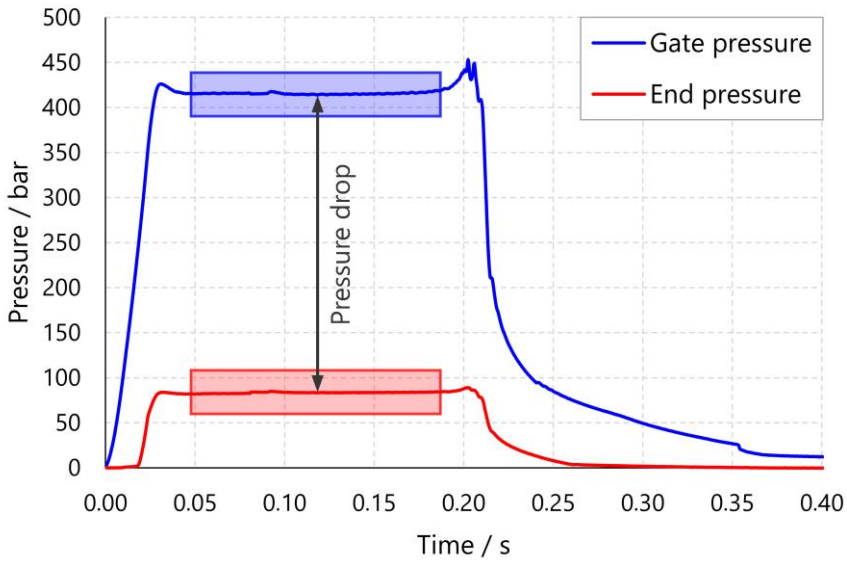

Fig. 2. Pressure signals acquired in the mold cavity by the piezoelectric transducers during polymer injection together with the resulting pressure drop.

2.6. Experimental approach

The effects of mold surface nano-structuring on melt flow resistance were investigated by conducting injection molding experiments under standard industrial processing conditions. In particular, the thermal conditions during the tests were non-isothermal as the mold surface temperature was significantly lower than the temperature of the injected polymer melt.

The effects of injection molding process parameters were evaluated by varying the injection speed and the mold temperature as shown in Table 3. In particular, the speed of the injection plunger was varied between 100 and 600 mm/s, which in turn caused the average velocity of the melt in the channel to range from 800 to 4900 mm/s.

Table 3. Injection molding process parameters selected for the experiments.

Parameter	Unit	Value
Injection Speed	mm/s	100, 200, 300, 450, 600
Mold Temperature	°C	60, 80
Melt Temperature	°C	230

In order to achieve adequate stability of the injection phase, 20 molding cycles were performed before the first acquisition of the cavity pressure. Then, 5 acquisitions were collected, one every 5 cycles, for each molding condition.

3. Numerical modelling

The slippage of the polymer melt over the LIPSS-treated mold cavity surfaces was modelled to understand the effect of different treatments on the pressure required to fill the thin-wall cavity. The governing equations for the 3-D flow simulation of a compressible viscous fluid under steady-state, non-isothermal and creeping flow conditions are given as follows. The continuity equation:

$$\frac{\partial \rho}{\partial t} + \nabla \cdot \rho \mathbf{v} = 0 \quad [1]$$

The momentum balance equation:

$$\rho \frac{D\mathbf{v}}{Dt} = \rho \mathbf{g} + \nabla \cdot \boldsymbol{\sigma} \quad [2]$$

The energy balance equation:

$$\rho c_p \left(\frac{\partial T}{\partial t} + \mathbf{v} \cdot \nabla T\right) = \beta T \left(\frac{\partial p}{\partial t} + \mathbf{v} \cdot \nabla p\right) + p \nabla \cdot \mathbf{v} + \boldsymbol{\sigma} : \nabla \mathbf{v} + \nabla \cdot (k \nabla T) \quad [3]$$

where ρ is the density, $\mathbf{v}$ is the velocity vector, p is the pressure, T is the temperature, c_p is the specific heat, β is the coefficient of volume expansion and $\boldsymbol{\sigma}$ is the stress tensor of the viscous fluid. The general relationship between the stress tensor and rate of the deformation tensor is $\boldsymbol{\sigma} = 2\eta(|\dot{\gamma}|)\mathbf{D}$. The rate of deformation tensor $\mathbf{D}$ is defined as: $\mathbf{D} = \left(\nabla \mathbf{v} + \nabla \mathbf{v}^{\mathbf{T}}\right)/2$, where $\nabla \mathbf{v}$ is the velocity gradient tensor. The well-known generalized non-Newtonian model described by the Cross–WLF equation was used to model the polymer viscosity:

$$\eta = \frac{\eta_0}{\left(1 + \frac{\eta_0 \dot{\gamma}}{\tau^*}\right)^{1-n}} \quad [4]$$

con

$$\eta_0 = D_1 e^{\left\{-\frac{A_1[T-(D_2+D_3 p)]}{\tilde{A}_2 + D_3 p + [T-(D_2+D_3 p)]}\right\}} \quad [5]$$

where n, τ^*, D_1, D_2, D_3, A_1 and $\tilde{A}_2$ are fitting parameters. The boundary conditions for the flow problem were constant flow rate at the gate and slip allowed boundary at the wall, governed by a modified power-law slip model by Rosenbaum and Hatzikiriakos [34]:

$$u_s = \frac{a}{1+\left(\frac{\sigma_c}{\sigma_w}\right)^k}\sigma_w^i \quad [6]$$

where u_s is the slip velocity, σ_w is wall shear stress, σ_c is the critical wall stress for slip, i is a power-law index, and a is a scalar coefficient. The factor $1 + \left(\frac{\sigma_c}{\sigma_w}\right)^k$ with a large power k basically zeros the slip velocity for stresses less than σ_c and it becomes about equal to one for shear stresses slightly greater than σ_c.

The thermal problem was relatively simple. The heat was considered to be transferred only across the mold wall. Viscous heating was included by the term $\eta\dot{\gamma}^2$. The boundary condition for the thermal problem was the Newton's equation for convective heat transfer:

$$\dot{Q} = hA(T_w - T_\infty) \quad [7]$$

where $\dot{Q}$ is the heat transferred per unit time, h is the heat transfer coefficient (*HTC*), A is the heat transfer surface area, T_w is the mold temperature and T_∞ is the melt temperature. In particular, a *HTC* value of 10,000 W/(m^{2}K) was used, which was determined by inverse analysis, fitting the results of a no-slip numerical simulation on the experimental ones for the untreated mold insert. Then, the numerical model was adjusted to the experimental data by introducing a slip velocity for the LIPSS-treated mold inserts. For the LIPSS-treated inserts the *HTC* was not varied but wall slip was introduced in the numerical model to account for the injection pressure reduction.

Process parameters in the simulation were set in agreement with those adopted for the experiments (Table 3). In particular, the flow rate filling control was set by calculating the time required for the polymer melt front to flow from the first to the second sensor in the cavity and thus to simulate accurately the flow conditions that characterize the polymer melt in the cavity [35].

4. Experimental results

4.1. LIPSS characterization

The mold surfaces covered with LIPSS were analyzed employing SEM and exhibited diverse orientation and morphology of the ripples (Fig. 3). In particular, the nano-structures are oriented along the flow direction for Insert 1, while they are similar but normal to the flow for Insert 2. Conversely, Insert 3 is characterized by crossed nano-structures, due to the two consecutive orthogonal laser scans. Thus, no significant LIPSS directionality for Insert 3 could be identified with respect to the flow direction,.

Overall, for the entire mold insert, the SEM analysis indicates good LIPSS homogeneity and absence of major defects over the whole surface that underwent a laser treatment.

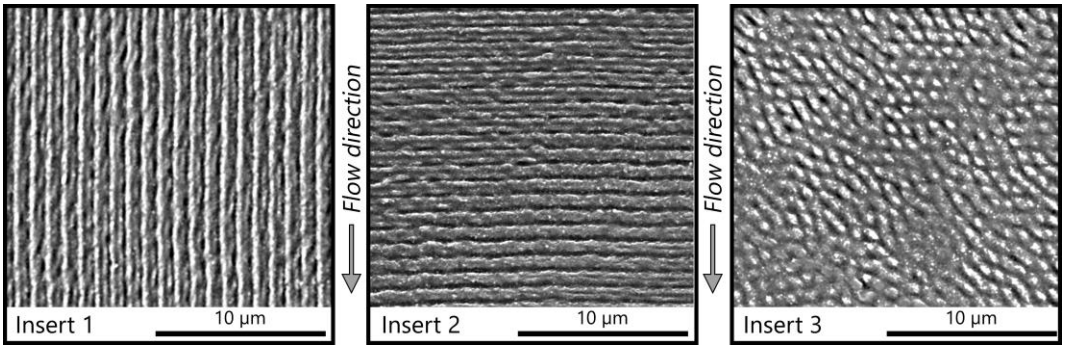

Fig. 3. SEM micrographs of the mold surfaces with the varying orientation of nano-structures.

Fig. 4 shows the ripples' topographies generated on the three different mold inserts together with respective profiles used to characterize their dimensions. Specifically, for each mold insert, the pitch, the width and the depth of the nano-structures were measured. The results of the analysis depicted in Table 4 show no significant dimensional difference between mold Insert 1 and Insert 2. Indeed, the topographies were generated by applying the same laser processing parameters and only the polarization plane was varied. The topographical characterization performed on Insert 3 indicates that the dimensions of the crossed-ripples are similar to those of the ripples' nano-structures realized on Insert 1 and Insert 2.

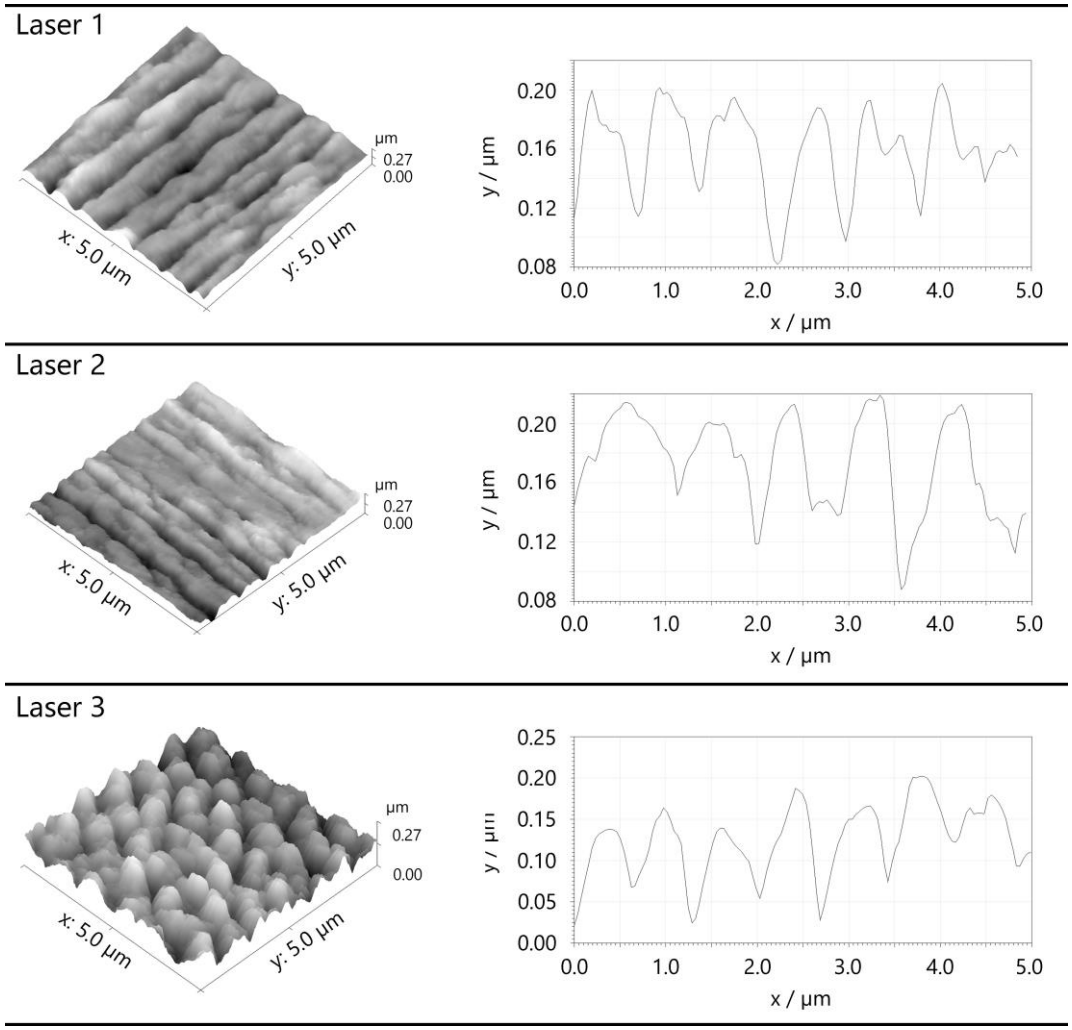

Fig. 4. AFM topographies and profiles of LIPSS on the three mold surfaces.

Table 4. AFM measurements of the nano-structures generated on the mold surfaces.

Treatment	Pitch [nm]		Width [nm]		Depth [nm]	
	Avg. Val.	Std. Dev.	Avg. Val.	Std. Dev.	Avg. Val.	Std. Dev.
Laser 1	742	134	784	82	87	38
Laser 2	791	104	758	145	89	23
Laser 3	747	100	759	54	109	13

4.2. Effect of LIPSS on drag reduction

The results of the injection molding experiments provide evidences that treating the mold surfaces with LIPSS can be effectively used to reduce the melt flow resistance. Fig. 5 (a) shows the effect of ripples on drag reduction

at a mold temperature of 60 °C and this is a clear evidence that all considered laser treatments had a positive effect. In particular, the highest reduction (i.e. 13%) was obtained with the intersecting ripples (Insert 3). Smaller, but still significant reductions, were observed for the parallel (i.e. 8%) and transversal (i.e. 3%) ripples.

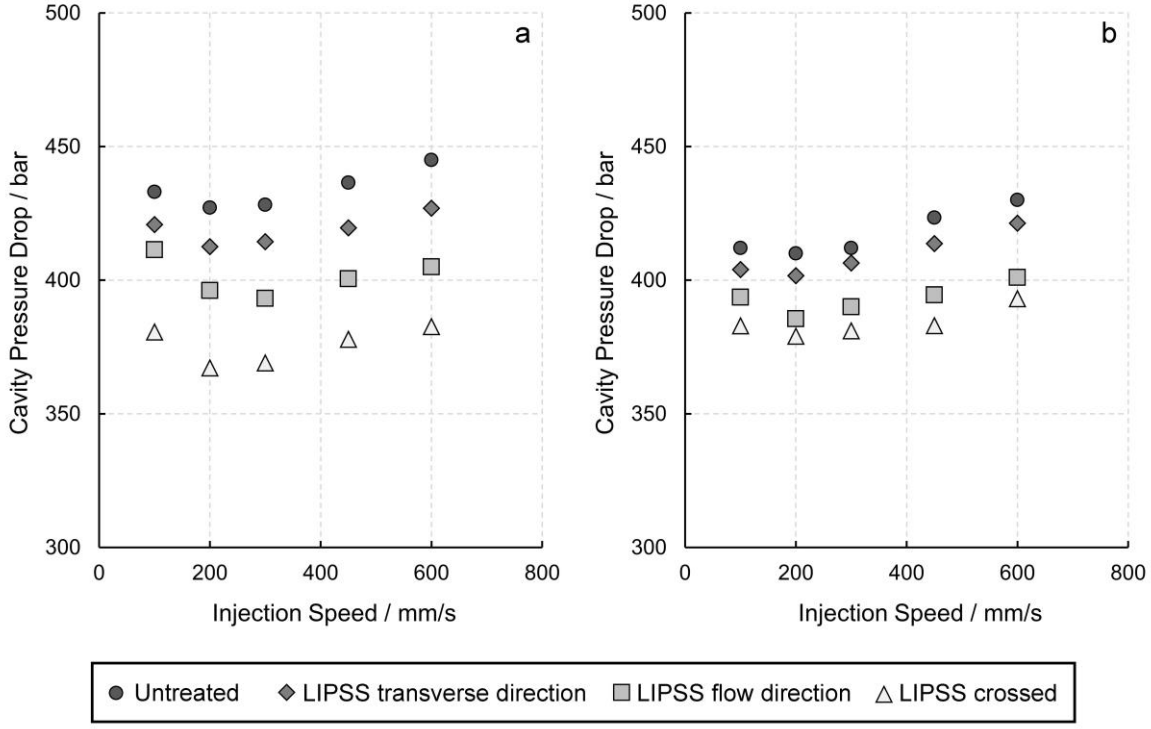

Fig. 5. Experimental measurements of cavity pressure drop (maximum standard deviation: 3 bar) for the three different LIPSS treatments as a function of the injection speed at mold temperature of (a) 60 °C and (b) 80°C.

Considering the influence of the LIPSS orientation on the pressure drop reduction, the filling flow of the polymer melt in the thin-wall cavity is clearly affected by the onset of the wall slip effect. In fact, a decrease of pressure drop due to the thermal insulation of the cavity would be less significant [11] and independent from the LIPSS orientation. Instead, the high viscosity of polypropylene and the low mold surface temperature when the cavity thickness was reduced led to high shear stresses at wall and a slippage of the polymer melt.

During the filling phase of the injection molding process, the polymer macromolecules in contact with the mold surface are adsorbed to it with a certain density, which is affected by the mold topography [32]. For a high

shear stress, above a critical value that depends on the density of adsorbed chains [36], the flow conditions are affected by the sudden disentanglement of the macromolecules in the bulk from those adsorbed at the interface. This leads to the formation of a polymer/polymer interface at which the strong slippage of the polymer melt occurs [12].

The nano-structured topographies generated on the mold inserts affect the slip phenomenon, and eventually the drag reduction, by modifying the adsorption density. In fact, due to the relatively low mold surface temperature, the macromolecules in the melt flow are not able to completely replicate the nano-scale LIPSS troughs and consequently the loop chains are adsorbed near ripples crests. Hence, the effect of the nano-structures is that of reducing the number of adsorption points at the mold surface in comparison with the untreated mold insert. The smaller resistance to disentanglement, due to lower adsorption density, lead to a lower value of the critical shear stress for the onset of a strong wall slip.

The highest reduction of the melt flow resistance was obtained with Insert 3, which is characterized by a topography that offers the less interaction with the filling polymer melt. The intersecting ripples favor the minimization of the areas where the macromolecules can be absorbed at the mold surface.

The different orientation of LIPSS in Insert 1 and Insert 2 did not modify the density of the adsorbed chains. However, under strong flow conditions, the transversal ripples obstruct the deformation of the macromolecules adsorbed at ripples crests by counteracting their bending, as observed by Sorgato et al. [32].

4.3. Effect of mold temperature

Fig. 5 (b) shows the effects of different LIPSS morphologies on drag reduction in the injection molding experiments carried out with a mold surface temperature of 80°C. Overall, it can be stated that a higher mold temperature reduces the effect of laser treatments in comparison with the results obtained at lower temperatures, i.e. at 60°C as discussed in the previous section. In particular, reductions of 6%, 2%, and 8%, were obtained with Insert 1, Insert2 and Insert 3, respectively.

The higher value of mold surface temperature reduces the thermal gradient between the mold surface and the polymer melt. Therefore, the polymer macromolecules can replicate better the nano-structured mold topography.

In fact, several researchers have reported that a higher mold temperature can be used to promote the replication of nano-structured topographies [37,38]. However, this increases the adsorption density at the polymer/mold interface that results in higher critical shear stress for the onset of the strong wall slip phenomenon.

5. Modelling of slip velocity

The results of the injection molding experiments indicate that the filling flow is affected by the wall slip phenomenon. In fact, when molding with the LIPSS treated inserts the pressure drop is smaller in comparison with that observed on the untreated mold insert. Hence, the higher the drag reduction the higher the slip velocity, due to the smaller interaction at the polymer/mold interface.

In order to evaluate the effect of the laser treatment on wall slip, a numerical model was calibrated by determining the slip velocity value that minimizes the difference between the simulated and experimental values. An inverse analysis approach was followed to carry out an iterative variation of the wall slip velocity in the numerical model.

Fig. 6 shows the results of the simulations, reporting the slip velocities calculated for the different LIPSS treatments as a function of the shear stress at wall. Since the wall slip model takes into account the pressure drop reduction measured on the LIPSS-treated inserts, a higher drag reduction corresponds to a higher slip velocity and therefore to a lower shear stress at wall. The high values of the calibrated slip velocity and their good linear correlation to the shear stress at wall indicate that, for all the experimental conditions, the flow conditions are in a strong-slip regime [39].

The results of the simulations provide further evidences that for higher mold temperatures the onset of the strong slip mechanism is shifted to higher values of the shear stress at the wall. Indeed, at 80 °C the higher adsorption density results in lower deformability of the macromolecules attached to cavity walls and thus in a higher resistance to their bending when under strong flow conditions [32].

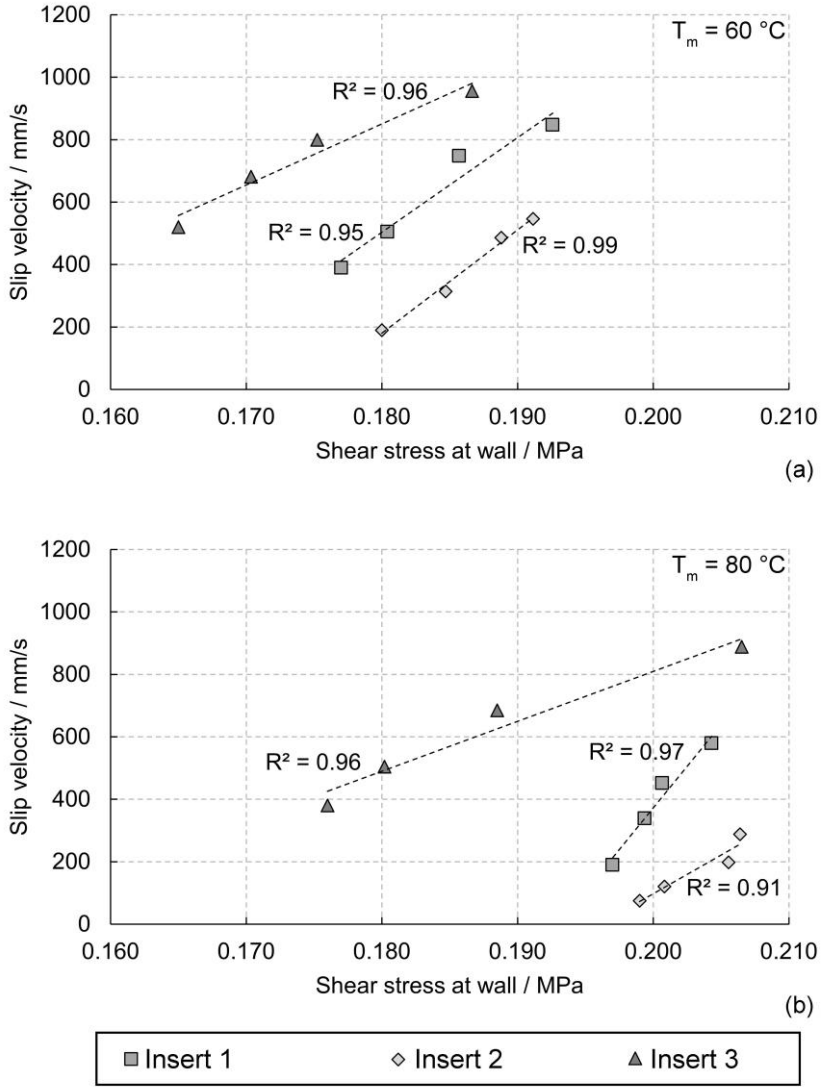

Fig. 6. Slip velocity of PP as a function of wall shear stress and LIPSS treatments for mold temperatures of (a) 60 °C and (b) 80 °C.

6. Conclusions

In this work, the effect of LIPSS on the filling flow resistance in thin-wall injection molding of polypropylene was investigated. The use of ultrafast laser processing of the mold surface allowed the generation of different surface topographies, which are characterized by nano-scale ripples of different orientation and morphology.

The results of the injection molding experiments showed that the different LIPSS topographies affect the filling resistance by modifying the critical shear stress in regards to the onset of the wall slip effect. In particular, nano-

structuring was observed to reduce the density of adsorbed macromolecules at the polymer/mold interface. The highest reduction of the injection pressure (i.e. 13%) was obtained when molding PP over the intersecting ripples. In fact, considering the reduced dimensions of the LIPSS troughs, the polymer is not able to replicate the nano-scale topographies and adsorption is limited near ripples intersections. Moreover, it was observed that the ripples parallel to the flow favors the bending of the adsorbed chain loops, and thus promoting the disentanglement from those adsorbed in the bulk in comparison with those normal to the flow.

The effect of laser treatment on wall slip was further investigated using a numerical model that was calibrated by determining the slip velocity value that minimizes the difference between the simulated and experimental values. In fact, the higher the drag reduction the higher the slip velocity, due to the smaller interaction at the polymer/mold interface. The good linear correlation between the calibrated slip velocity values and the shear stress at wall, obtained from the simulations, shows that the flow conditions are characterized by a strong slip regime.

The effect of increasing the mold surface temperature was investigated both experimentally and numerically. The results show that the LIPSS treatment affects the filling flow by shifting the onset of the strong slip phenomenon to higher shear stress values. Indeed, the higher adsorption density at a higher temperature results in lower deformability of the macromolecules attached to cavity walls and thus in a higher resistance to their bending when under strong flow conditions.

Funding

This research did not receive any specific grant from funding agencies in the public, commercial, or not-for-profit sectors.

References

[1] Thiriez, A., & Gutowski, T. (2006, May). An environmental analysis of injection molding. In Electronics and the Environment, 2006. Proceedings of the 2006 IEEE International Symposium on (pp. 195-200). IEEE.

[2] Yao, D., & Kim, B. (2002). Increasing flow length in thin wall injection molding using a rapidly heated mold. Polymer-Plastics Technology and Engineering, 41(5), 819-832.

[3] Song, M. C., Liu, Z., Wang, M. J., Yu, T. M., & Zhao, D. Y. (2007). Research on effects of injection process parameters on the molding process for ultra-thin wall plastic parts. Journal of Materials Processing Technology, 187, 668-671.

[4] Lucchetta, G., & Bariani, P. F. (2010). Sustainable design of injection moulded parts by material intensity reduction. CIRP Annals-Manufacturing Technology, 59(1), 33-36.

[5] Giboz, J., Copponnex, T., & Mélé, P. (2007). Microinjection molding of thermoplastic polymers: a review. Journal of micromechanics and microengineering, 17(6), R96.

[6] Masato, D., Sorgato, M., Parenti, P., Annoni, M., & Lucchetta, G. (2017). Impact of deep cores surface topography generated by micro milling on the demolding force in micro injection molding. Journal of Materials Processing Technology, 246, 211-223.

[7] Griffiths, C. A., Dimov, S. S., Scholz, S., Hirshy, H., & Tosello, G. (2011). Process factors influence on cavity pressure behavior in microinjection moulding. Journal of Manufacturing Science and Engineering, 133(3), 031007.

[8] Griffiths, C. A., Dimov, S. S., Brousseau, E. B., & Hoyle, R. T. (2007). The effects of tool surface quality in micro-injection moulding. Journal of Materials Processing Technology, 189(1-3), 418-427.

[9] Masato, D., Sorgato, M., Babenko, M., Whiteside, B., & Lucchetta, G. (2018). Thin-wall injection molding of polystyrene parts with coated and uncoated cavities. Materials & Design, 141, 286-295.

[10] Zhang, N., & Gilchrist, M. D. (2012). Characterization of thermo-rheological behavior of polymer melts during the micro injection moulding process. Polymer testing, 31(6), 748-758.

[11] Lucchetta, G., Masato, D., Sorgato, M., Crema, L., & Savio, E. (2016). Effects of different mould coatings on polymer filling flow in thin-wall injection moulding. CIRP Annals-Manufacturing Technology, 65(1), 537-540.

[12] Ebrahimi, M., Konaganti, V. K., Moradi, S., Doufas, A. K., & Hatzikiriakos, S. G. (2016). Slip of polymer melts over micro/nano-patterned metallic surfaces. Soft Matter, 12(48), 9759-9768.

[13] Joshi, Y. M., Lele, A. K., & Mashelkar, R. A. (2000). A unified wall slip model. Journal of Non-Newtonian Fluid Mechanics, 94(2-3), 135-149.

[14] Mhetar, V., & Archer, L. A. (1998). Slip in entangled polymer melts. 2. Effect of surface treatment. Macromolecules, 31(24), 8617-8622.

[15] Wang, S. Q., & Drda, P. A. (1997). Stick-slip transition in capillary flow of linear polyethylene: 3. Surface conditions. Rheologica Acta, 36(2), 128-134.

[16] Sanchez-Reyes, J., & Archer, L. A. (2003). Interfacial slip violations in polymer solutions: Role of microscale surface roughness. Langmuir, 19(8), 3304-3312.

[17] Bellantone, V., Surace, R., Modica, F., & Fassi, I. (2018). Evaluation of mold roughness influence on injected thin micro-cavities. The International Journal of Advanced Manufacturing Technology, 94(9-12), 4565-4575.

[18] Zhang, H. L., Ong, N. S., & Lam, Y. C. (2007). Effects of surface roughness on microinjection molding. Polymer Engineering & Science, 47(12), 2012-2019.

[19] Bonse, J., Höhm, S., Kirner, S. V., Rosenfeld, A., & Krüger, J. (2017). Laser-induced periodic surface structures—a scientific evergreen. IEEE Journal of Selected Topics in Quantum Electronics, 23(3), 109-123.

[20] Orazi, L., Gnilitskyi, I., Pavlov, I., Serro, A. P., Ilday, S., & Ilday, F. O. (2015). Nonlinear laser lithography to control surface properties of stainless steel. CIRP Annals-Manufacturing Technology, 64(1), 193-196.

[21] Wu, B., Zhou, M., Li, J., Ye, X., Li, G., & Cai, L. (2009). Superhydrophobic surfaces fabricated by microstructuring of stainless steel using a femtosecond laser. Applied Surface Science, 256(1), 61-66.

[22] Bizi-Bandoki, P., Benayoun, S., Valette, S., Beaugiraud, B., & Audouard, E. (2011). Modifications of roughness and wettability properties of metals induced by femtosecond laser treatment. Applied Surface Science, 257(12), 5213-5218.

[23] Bhaduri, D., Batal, A., Dimov, S. S., Zhang, Z., Dong, H., Fallqvist, M., & M'saoubi, R. (2017). On design and tribological behaviour of laser textured surfaces. Procedia CIRP, 60, 20-25.

[24] Garcia-Giron, A., Romano, J. M., Liang, Y., Dashtbozorg, B., Dong, H., Penchev, P., & Dimov, S. S. (2018). Combined surface hardening and laser patterning approach for functionalising stainless steel surfaces. Applied Surface Science, 439, 516-524.

[25] Šugárová, J., Šugár, P., Frnčík, M., Necpal, M., Moravčíková, J., & Kusý, M. (2018). The Influence of the Tool Surface Texture on Friction and the Surface Layers Properties of Formed Component. Advances in Science and Technology. Research Journal, 12(1), 181-193.

[26] Wu, P. H., Cheng, C. W., Chang, C. P., Wu, T. M., & Wang, J. K. (2011). Fabrication of large-area hydrophobic surfaces with femtosecond-laser-structured molds. Journal of Micromechanics and Microengineering, 21(11), 115032.

[27] Romano, J. M., Gulcur, M., Garcia-Giron, A., Martinez-Solanas, E., Whiteside, B. R., & Dimov, S. S. (2019). Mechanical durability of hydrophobic surfaces fabricated by injection moulding of laser-induced textures. Applied Surface Science.

[28] Bekesi, J., Kaakkunen, J. J. J., Michaeli, W., Klaiber, F., Schoengart, M., Ihlemann, J., & Simon, P. (2010). Fast fabrication of super-hydrophobic surfaces on polypropylene by replication of short-pulse laser structured molds. Applied Physics A, 99(4), 691-695.

[29] Jwad, T., Penchev, P., Nasrollahi, V., & Dimov, S. (2018). Laser induced ripples' gratings with angular periodicity for fabrication of diffraction holograms. Applied Surface Science, 453, 449-456.

[30] Menotti, S., Hansen, H. N., Bissacco, G., Calaon, M., Tang, P. T., & Ravn, C. (2014). Injection molding of nanopatterned surfaces in the sub-micrometer range with induction heating aid. The International Journal of Advanced Manufacturing Technology, 74(5-8), 907-916.

[31] Masato, D., Sorgato, M., & Lucchetta, G. (2016). Analysis of the influence of part thickness on the replication of micro-structured surfaces by injection molding. Materials & Design, 95, 219-224.

[32] Sorgato, M., Masato, D., Lucchetta, G., & Orazi, L. (2018). Effect of different laser-induced periodic surface structures on polymer slip in PET injection moulding. CIRP Annals-Manufacturing Technology, 67(1), 575-578.

[33] Laun, H. M. (1983). Polymer melt rheology with a slit die. Rheologica Acta, 22(2), 171-185.

[34] Rosenbaum, E. E. & Hatzikiriakos, S. G. (1997). Wall slip in the capillary flow of molten polymers subject to viscous heating. AIChE Journal, 43, 598–608

[35] Zhang, N., & Gilchrist, M. D. (2012). Characterization of thermo-rheological behavior of polymer melts during the micro injection moulding process. Polymer Testing, 31(6), 748-758.

[36] Hatzikiriakos, S. G. (2012). Wall slip of molten polymers. Progress in Polymer Science, 37(4), 624-643.

[37] Chen, S. C., Jong, W. R., Chang, Y. J., Chang, J. A., & Cin, J. C. (2006). Rapid mold temperature variation for assisting the micro injection of high aspect ratio micro-feature parts using induction heating technology. Journal of Micromechanics and Microengineering, 16(9), 1783.

[38] Lucchetta, G., Fiorotto, M., & Bariani, P. F. (2012). Influence of rapid mold temperature variation on surface topography replication and appearance of injection-molded parts. CIRP Annals-Manufacturing Technology, 61(1), 539-542.

[39] Mhetar, V., & Archer, L. A. (1998). Slip in entangled polymer melts. 1. General features. Macromolecules, 31(24), 8607-8616.